Supporting Information

Metal-Free Visible-Light Photoactivated C_3N_4 Bubble-Propelled Tubular Micromotors with Inherent Fluorescence and On/Off Capabilities

Katherine Villa[†], C. Lorena Manzanares Palenzuela[†], Zdeněk Sofer[†], Stanislava Matějková[§] and Martin Pumera[†]*

† Department of Inorganic Chemistry, University of Chemistry and Technology Prague, Technická 5, 1668 28 Prague, Czech Republic.

§ Institute of Organic Chemistry and Biochemistry of the CAS, Flemingovo nám. 542/2, 166 10 Prague, Czech Republic.

* Author for correspondence: M. Pumera; email: pumera.research@gmail.com

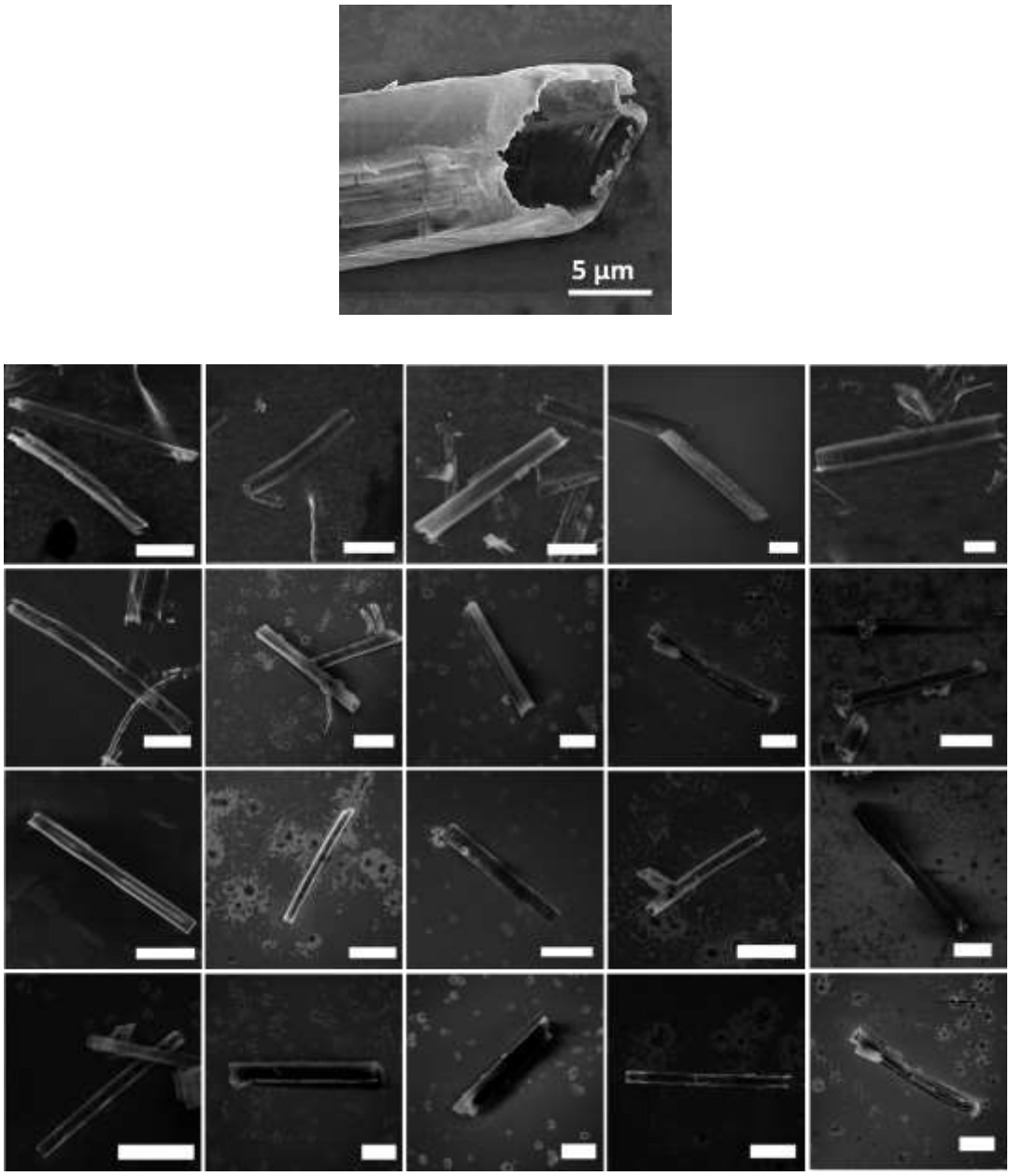

Figure S1. SEM image of the tube cavity of a GCN micromotor (above) and SEM images of different micromotors, showing their size distribution (below), scale bars: 20 µm.

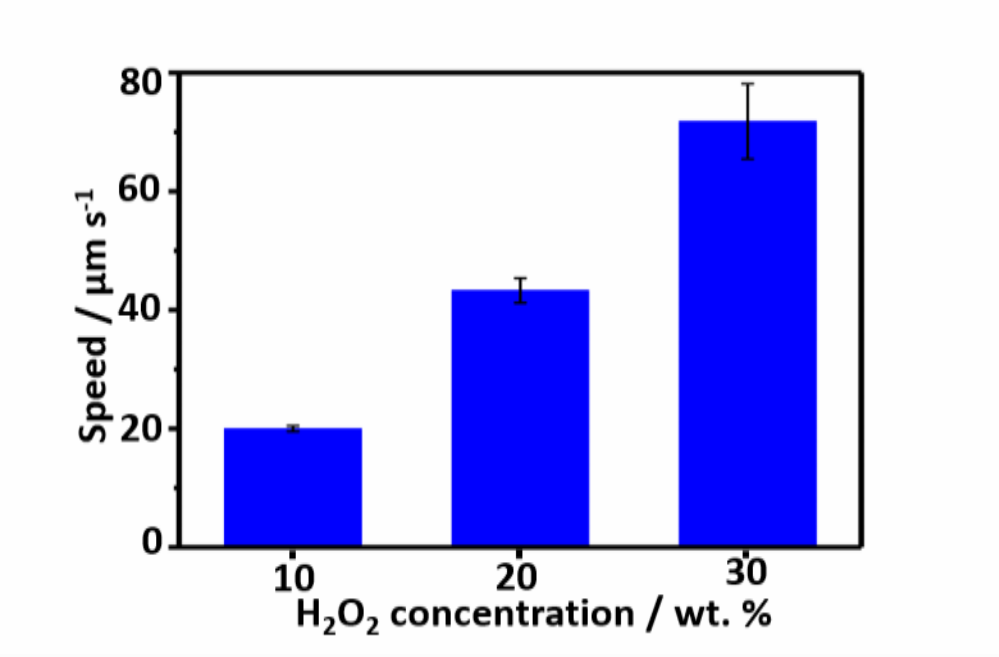

Figure S2. Speed of GCN micromotors at different H_2O_2 concentrations (n=7, error bars represent the standard error of the mean).

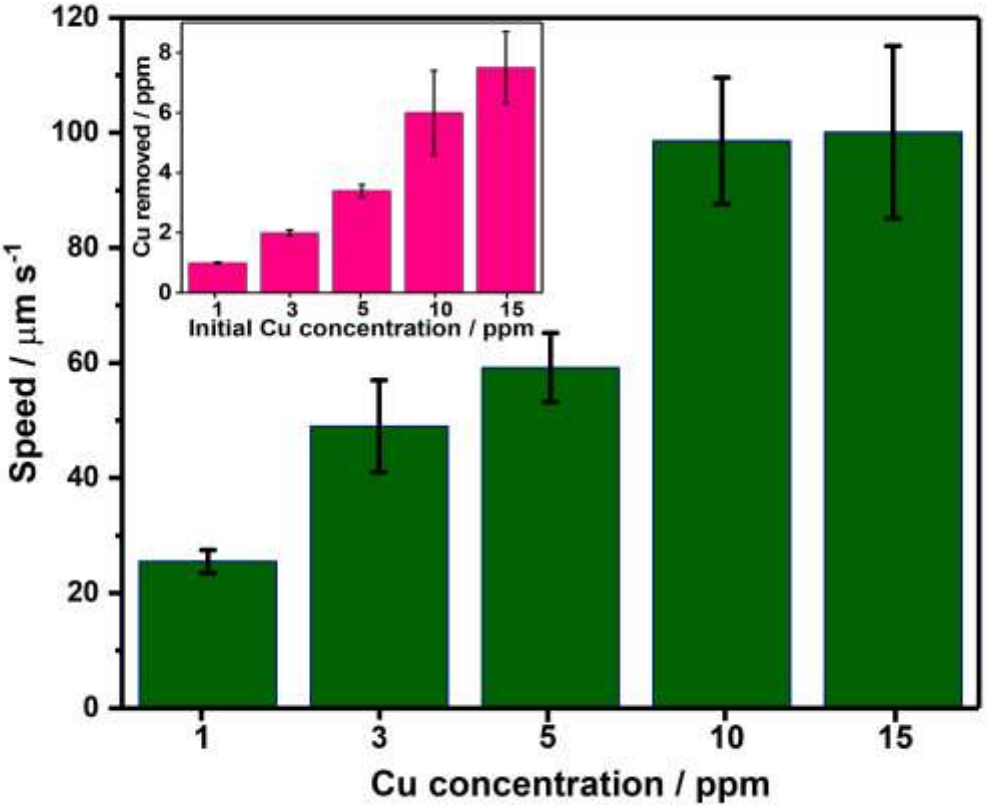

Figure S3. Speed of GCN micromotors at a 5 wt.% H_2O_2 concentration, 0.25 wt. % SDS and different Cu concentrations (1, 3, 5, 10 and 15 ppm) (n=7, error bars represent the standard error of the mean). Inset corresponds to the Cu removal efficiency of GCN micromotors in the presence of different Cu concentrations (1, 3, 5, 10 and 15 ppm) (n=2, error bars represent the standard error of the mean).

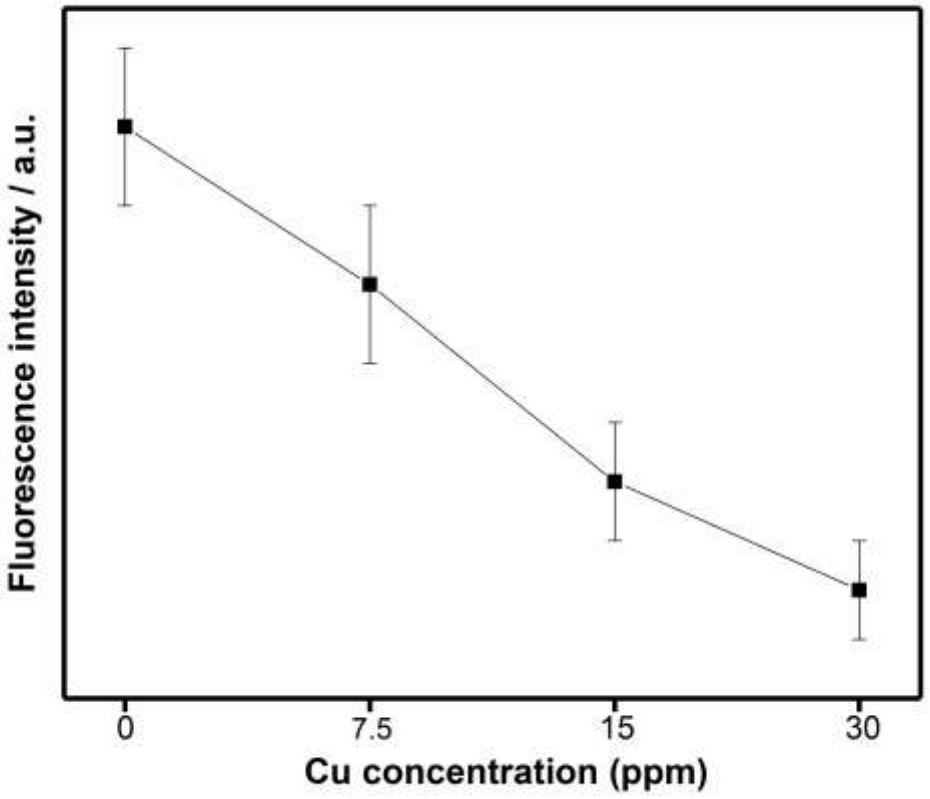

Figure S4. Fluorescence intensity decay of GCN micromotors in the presence of different Cu concentrations by fluorescent optical microscopy (n=10, error bars represent the standard error of the mean). The fluorescence intensity was estimated by Image pro 9 software.

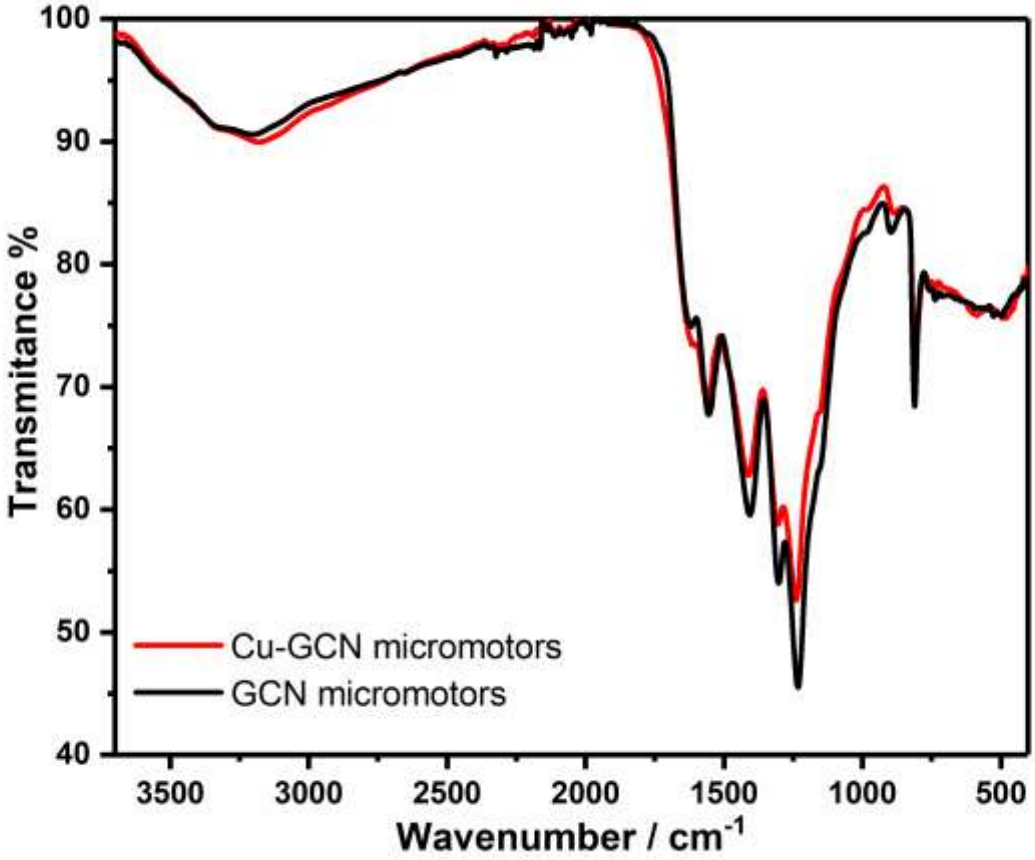

Figure S5. FTIR spectra of GCN micromotors before and after adsorption of Cu^{2+} ions.

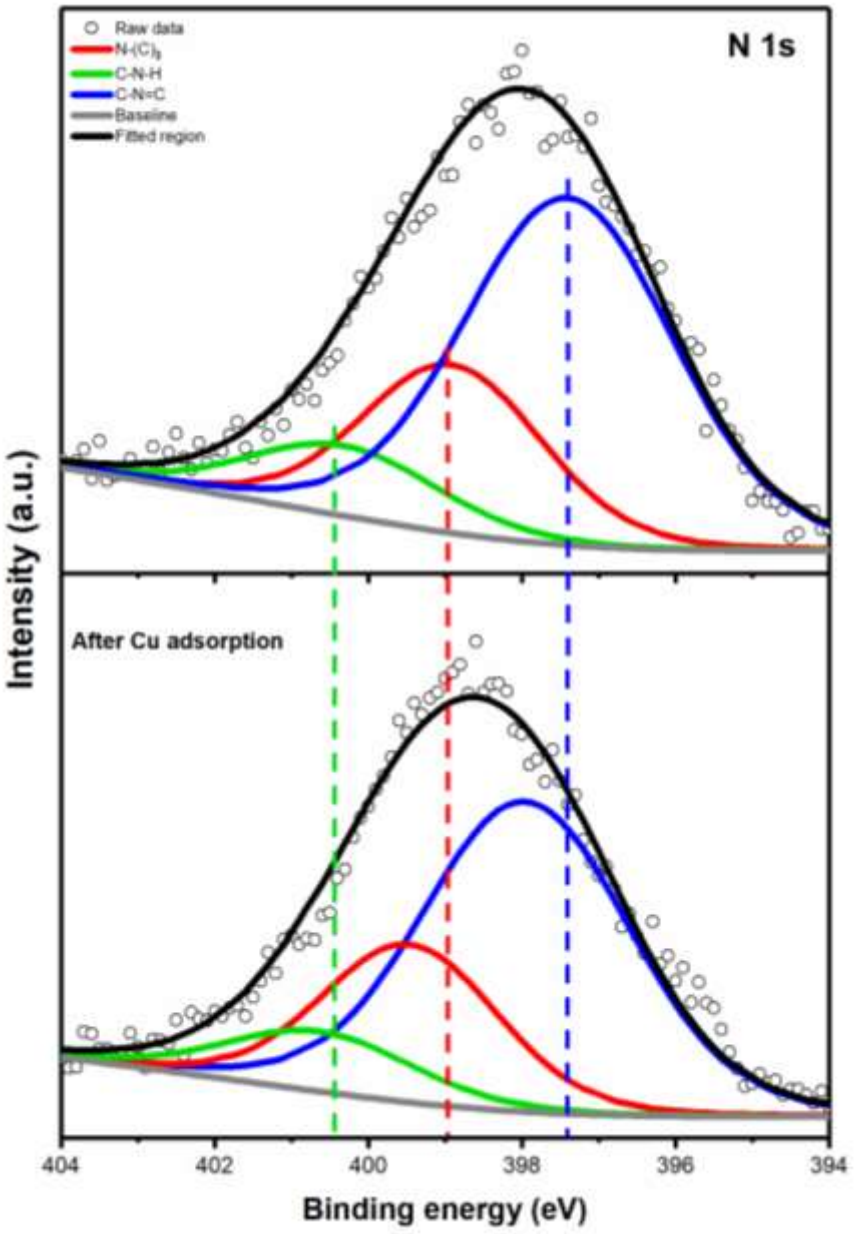

Figure S6. XPS spectra (N 1s region) of GCN micromotors before and after adsorption of Cu^{2+} ions.

Micromotor	Shape	Motion mechanism	Light source	Speed (μm s^{-1})	Reference
TiO_2/Pt	Sphere	Self-electrophoresis	UV	9.7	[1]
TiO_2/Au	Sphere	Self-electrophoresis	UV	25.0	[2]
TiO_2/Si	Nanotree	Self-electrophoresis	UV	6.0	[3]
WO_3/Au	Sphere	Self-diffusiophoresis	UV	16.0	[4]
ZnO/Pt	Tubular	Bubble-propelled	UV	512.0	[5]
TiO_2	Tubular	Bubble-propelled	UV	325.0	[6]
g-C_3N_4/Pt	Sphere	Self-diffusiophoresis	UV	23	[7]
TiO_2-Au/B	Sphere	Self-electrophoresis	Visible	10.0	[8]
Si/Au	Microrods	Self-electrophoresis	Visible	5	[9]
BiOI/Au	Sphere	Self-electrophoresis	Visible	1.62	[10]
CuO_2/Au	Sphere	Self-electrophoresis	Visible	6.0	[11]
g-C_3N_4	Tubular	Bubble-propelled	Visible	72	This work
Non-photocatalytic micromotors					
Ti/Au−catalase	Tubular	Bubble-propelled	---	226	[12]
Pedot/Au-catalase	Tubular	Bubble-propelled	---	130	[13]

Table S1. Motion mechanism, light source and speed comparison of different light-driven photocatalytic-based micromotors and non-photocatalytic micromotors based on enzymes.

References

(1) Kong, L.; Mayorga-Martinez, C. C.; Guan, J.; Pumera, M. Fuel-Free Light-Powered TiO_2/Pt Janus Micromotors for Enhanced Nitroaromatic Explosives Degradation. *ACS Appl. Mater. Interfaces* **2018**, *10*, 22427–22434.

(2) Dong, R.; Zhang, Q.; Gao, W.; Pei, A.; Ren, B. Highly Efficient Light-Driven TiO_2–Au Janus Micromotors. *ACS Nano* **2016**, *10*, 839–844.

(3) Dai, B.; Wang, J.; Xiong, Z.; Zhan, X.; Dai, W.; Li, C.-C.; Feng, S.-P.; Tang, J. Programmable Artificial Phototactic Microswimmer. *Nat. Nanotechnol.* **2016**, *11*, 1087–1092.

(4) Zhang, Q.; Dong, R.; Wu, Y.; Gao, W.; He, Z.; Ren, B. Light-Driven Au-WO_3@C Janus Micromotors for Rapid Photodegradation of Dye Pollutants. *ACS Appl. Mater. Interfaces* **2017**, *9*, 4674–4683.

(5) Dong, R.; Wang, C.; Wang, Q.; Pei, A.; She, X.; Zhang, Y.; Cai, Y. ZnO-Based Microrockets with Light-Enhanced Propulsion. *Nanoscale* **2017**, *9*, 15027–15032.

(6) Mou, F.; Li, Y.; Chen, C.; Li, W.; Yin, Y.; Ma, H.; Guan, J. Single-Component TiO_2 Tubular Microengines with Motion Controlled by Light-Induced Bubbles. *Small* **2015**, *11*, 2564–2570.

(7) Ye, Z.; Sun, Y.; Zhang, H.; Song, B.; Dong, B. A Phototactic Micromotor Based on Platinum Nanoparticle Decorated Carbon Nitride. *Nanoscale* **2017**, *9*, 18516–18522.

(8) Jang, B.; Hong, A.; Kang, H. E.; Alcantara, C.; Charreyron, S.; Mushtaq, F.; Pellicer, E.; Büchel, R.; Sort, J.; Lee, S. S.; Nelson, B. J.; Pané, S. Multiwavelength Light-Responsive Au/B-TiO_2 Janus Micromotors. *ACS Nano* **2017**, *11*, 6146–6154.

(9) Zhou, D.; Li, Y. C.; Xu, P.; Ren, L.; Zhang, G.; Mallouk, T. E.; Li, L. Visible-Light Driven Si–Au Micromotors in Water and Organic Solvents. *Nanoscale* **2017**, *9*, 11434–11438.

(10) Dong, R.; Hu, Y.; Wu, Y.; Gao, W.; Ren, B.; Wang, Q.; Cai, Y. Visible-Light-Driven BiOI-Based Janus Micromotor in Pure Water. *J. Am. Chem. Soc.* **2017**, *139*, 1722–1725.

(11) Zhou, D.; Li, Y. C.; Xu, P.; McCool, N. S.; Li, L.; Wang, W.; Mallouk, T. E. Visible-Light Controlled Catalytic Cu_2O–Au Micromotors. *Nanoscale* **2016**, *9*, 75–78.

(12) Sanchez, S.; Solovev, A. A.; Mei, Y.; Schmidt, O. G. Dynamics of Biocatalytic Microengines Mediated by Variable Friction Control. *J. Am. Chem. Soc.* **2010**, *132*, 13144–13145.
(13) Orozco, J.; García-Gradilla, V.; D'Agostino, M.; Gao, W.; Cortés, A.; Wang, J. Artificial Enzyme-Powered Microfish for Water-Quality Testing. *ACS Nano* **2013**, *7*, 818–824.